Separation of Agile Waveform Time-Frequency Signatures from Coexisting Multimodal Systems

by

Vineet Sunil Gattani

A Thesis Presented in Partial Fulfillment
of the Requirements for the Degree
Master of Science

Approved November 2018 by the
Graduate Supervisory Committee:

Antonia Papandreou-Suppappola, Chair
Christ Richmond
Alexander Maurer

ARIZONA STATE UNIVERSITY

December 2018

ABSTRACT

As the demand for wireless systems increases exponentially, it has become necessary for different wireless modalities, like radar and communication systems, to share the available bandwidth. One approach to realize coexistence successfully is for each system to adopt a transmit waveform with a unique nonlinear time-varying phase function. At the receiver of the system of interest, the waveform received for processing may still suffer from low signal-to-interference-plus-noise ratio (SINR) due to the presence of the waveforms that are matched to the other coexisting systems. This thesis uses a time-frequency based approach to increase the SINR of a system by estimating the unique nonlinear instantaneous frequency (IF) of the waveform matched to the system. Specifically, the IF is estimated using the synchrosqueezing transform, a highly localized time-frequency representation that also enables reconstruction of individual waveform components. As the IF estimate is biased, modified versions of the transform are investigated to obtain estimators that are both unbiased and also matched to the unique nonlinear phase function of a given waveform. Simulations using transmit waveforms of coexisting wireless systems are provided to demonstrate the performance of the proposed approach using both biased and unbiased IF estimators.

To my parents

ACKNOWLEDGEMENTS

I would like to thank Dr. Antonia Papandreou-Suppappola for her continued guidance, support and encouragement throughout my work.

I would also like to thank my committee members, Dr. Christ Richmond and Dr. Alexander Maurer, for their valuable participation in this thesis.

This work was partly supported by the Air Force Office of Scientific Research Grant FA9550-17-1-0100.

TABLE OF CONTENTS

CHAPTER Page

LIST OF FIGURES

Figure Page

Chapter 1

INTRODUCTION

1.1 Motivation

In a multimodal sensing system, it is often necessary for different wireless modalities to share the available bandwidth to avoid spectrum congestion. An example of a multimodal environment with joint wireless radar and communications systems is depicted in Figure 1.1. In order to enable spectrum sharing, the signaling scheme of one system must be appropriately designed to minimize the high interference caused by the other system. Recently, various such methods have been considered for coexisting radar and communication systems. In [2], for example, the radar transmit waveform was optimized using constraints on desirable levels of signal-to-interference-plus-noise ratio (SINR) and radar power, whereas in [3], low-probability of intercept communications symbols were designed for high-power radar emissions. A radar waveform selection approach was considered in [4, 5] based on the waveform-dependent SINR threshold. In particular, the radar transmit waveforms were designed to have nonlinear time-frequency (TF) signatures which were different from the linear TF signatures of the waveforms normally used in wireless systems. At the receiver of the system of interest, the received signal consisted of not only the system-matched waveform but also interference due to the waveforms from the other systems. Knowledge of the system's transmit waveform unique TF characteristics is used at the receiver to design waveform agile processing methods to increase the system's overall performance. However, depending on the level of SINR, the problem of spectrum congestion may not be completely resolved and pre-processing methods may need to be designed.

Figure 1.1: Illustration of a multimodal environment with joint radar and communications systems. (The figure is taken from [1])

1.2 Proposed Work

Although waveform agile sensing methods have been used to enable spectrum coexistence of wireless systems, system performance can be further increased using TF pre-processing methods. In particular, as coexisting systems are designed to have transmit waveforms with unique TF signatures, an appropriately designed TF method could be used to separate a multicomponent received waveform into its components. Such a TF method must be very highly localized in both time and frequency in order to distinctively differentiate between TF signatures present in a waveform. The method must also be able to accurately reconstruct individual components present in a multicomponent waveform. In order to demonstrate the need for a method that can provide very high TF resolution, assume that we have a coexisting radar and communications multimodal system. The radar system of interest uses hyperbolic frequency-modulated (FM) transmit waveforms, whereas the transmit waveforms of communication users, that appear as high interference to the radar, are linear FM waveforms. At the radar receiver, a TF pre-processing method must be designed to resolve the nonlinear hyperbolic instantaneous frequency (IF) from the multiple linear IFs that correspond to the communications interference before further processing at the receiver. An illustration of such multiple IFs sharing the same spectrum in the TF

plane is demonstrated in Figure 1.2. As it can be seen, there are two different unique TF signatures present, and high TF localization is essential for potential waveform separation. Note that Figure 1.2 was obtained using the MATLAB Time-Frequency Toolbox freeware [6]. The plot shows an ideal TFR formed as the linear combination of the IFs of a hyperbolic FM and three linear FM waveforms. The IF is not a linear representation, so the TF plot does not represent the IF of the sum of the waveforms.

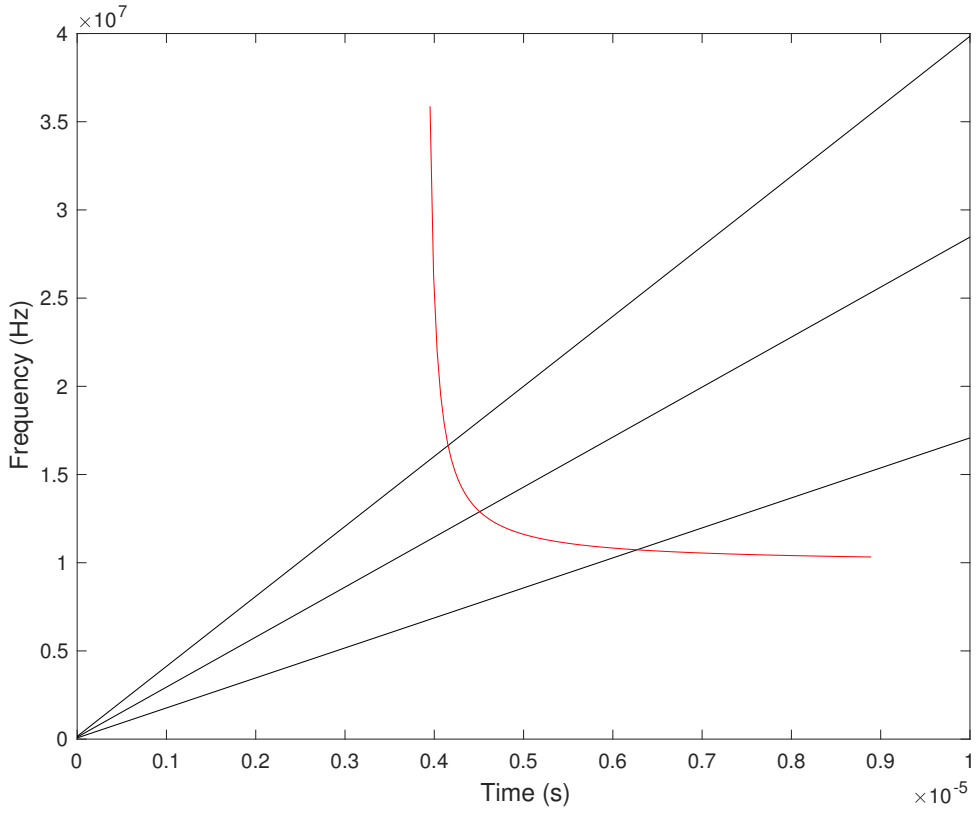

Figure 1.2: Ideal TF representation of a hyperbolic FM and three linear FM waveforms sharing the same bandwidth in a coexisting system.

The TF method we consider is based on the synchrosqueezing transform (SST), a TF representation (TFR) that has been shown to be robust to bounded signal per-

turbations and additive white Gaussian noise. A synchrosqueezing wavelet transform was first developed by Maes and Daubechies in [7] and then extended by Flandrin to the SST that is based on the short-time Fourier transform linear TFR [8–11]. The SST is highly localized in both time and frequency. In addition, it provides a natural framework for reconstructing multicomponent waveforms into their linearly combined components that consist of waveforms with linear or nonlinear phase functions [12]. Under certain conditions, the SST can be used to separate the components and provide an accurate estimate of the IFs of the waveforms. One of these conditions is that the waveform components must have low frequency modulation. In particular, it has been shown in [13] that the SST provides a biased estimate of the IFs of the waveforms with high frequency modulation. In [13], versions of the synchrosqueezing transform using different unbiased IF estimators were developed that are better matched to high frequency modulation. Note, however, that these modified SST transforms are only matched to linear FM waveforms.

In this work, we propose new modified SST TFRs that are matched to waveforms with nonlinear IFs. In particular, these TFRs can be used to provide unbiased estimates of IFs that are highly nonlinear, such as hyperbolic or power functions. If a multicomponent waveform consists of both linear FM and hyperbolic FM waveforms, for example, then only the new proposed TFR, appropriately designed to match hyperbolic TF signatures, can provide an unbiased IF as well as separate the hyperbolic waveform component from the overall waveform. We derive the conditions needed on the nonlinear IF function in order for the corresponding matched SST to yield an unbiased IFE. We also demonstrate that these conditions are in agreement with existing signaling schemes in coexisting multimodal systems for minimizing system interference.

A matched unbiased SST can also be used as a pre-processing TF filtering ap-

proach for reducing the number of false alarms at a radar receiver when only communications signals are present in the received signal. It could also be used to determine the time frame that contains the radar received signal to reduce receiver processing time.

Part of this work was published in [14].

1.3 Thesis Organization

This thesis is organized as follows. Chapter 2 provides some background on various TFRs and their localization properties in time and frequency. In particular, it discusses the reassignment method that is a TFR with high TF resolution properties but fails in signal reconstruction. This chapter also introduces the synchrosqueezing transform (SST) as a TFR that not only satisfies high TF resolution properties but it can also achieve signal reconstruction. The SST can be used to obtain a biased instantaneous frequency estimate (IFE) of the linearly combined components of a multicomponent waveform, as also discussed in Chapter 2. In Chapter 3, a modified SST is examined that can be used to obtain unbiased IFEs but only for linear FM waveforms. In Chapter 4, we present our proposed modified SST that can be used to obtain unbiased IFEs for signals with nonlinear IF. This chapter demonstrates the performance of both the the SST and the modified SST to obtain IFEs under varying SINR conditions. We also consider a realistic scenario of a wireless coexisting multimodal system consisting of a radar transmitting a waveform with nonlinear IF and a communications system transmitting a waveform with linear IF. Chapter 5 summarizes our results and discusses future research directions.

In this thesis, we use the terms signal and waveform interchangeably to refer to a function that conveys information.

Chapter 2

WAVEFORM LOCALIZATION IN TIME AND FREQUENCY

Time-frequency representations (TFRs) are processing methods for analyzing time-varying or non-stationary signals; these are signals whose frequency content changes with time. In particular, a TFR can convey information about the time-varying characteristics of each frequency component present in a given signal. TFRs can be broadly classified into linear and quadratic signal transformations. The most commonly used linear TFR is the short-time Fourier transform (STFT), whereas some quadratic TFRs include the spectrogram and the Wigner distribution [15, 16].

2.1 Linear and Quadratic Time-Frequency Representations

The STFT of a signal $x(t)$, $t \in \mathcal{R}$, is formed by taking the Fourier transform (FT) of time-shifted windowed segments of the signal. Using an analysis window $g(t)$ [17], the STFT is defined as

$$S_x(t, f; g) = \int x(\tau)\, g(\tau - t)\, e^{-j2\pi f \tau} d\tau\,. \tag{2.1}$$

Due to the ease of its implementation, the STFT is commonly used in many applications. However, the STFT often provides incorrect information on the analysis signal because its time-frequency (TF) localization is highly dependent on the selection of its window. Specifically, the duration of the window determines the TF resolution of the representation: a window with a short duration provides a highly localized transform in time, whereas a window with a long duration provides a highly localized transform in frequency. This follows from the uncertainty principle that states that it is not possible to perfectly localize a signal in both time and frequency [15].

Figure 2.1 shows the TF resolution trade-off of the STFT as a result of varying the duration of its window during signal analysis. In particular, the spectrogram (magnitude-squared of the STFT) is used to analyze the sum of two Gaussian signals, each of duration 1 second and bandwidth 1 kHz. The window used in (2.1) is $g(t) = e^{-\pi t^2/\sigma^2}$ with duration T_g; the sampling frequency used is $f_s = 2.5$ kHz. In Figures 2.1(a) and 2.1(b), the duration of the window was increased from 0.13 s to 0.5 s, respectively. As it can be observed, when the long duration window is used in Figure 2.1(b), the high frequency resolution of the STFT results in the two Gaussian signals appearing as one constant frequency signal, thus providing incorrect information. As in this example, the STFT trade-off in TF resolution due to the window duration may not always yield satisfactory analysis results.

The squared-magnitude of the STFT results in the spectrogram quadratic TFR, that is given by

$$\mathrm{SP}_x(t, f; g) = \mid S_x(t, f; g) \mid^2 \ .$$

The spectrogram has the advantage of removing any phase information or negative components.

Another well-known quadratic TFR is the Wigner distribution (WD), which, for a signal $x(t)$, $t \in \mathcal{R}$, is defined as

$$W_x(t, f) = \int x\Big(t + \frac{\tau}{2}\Big)\, x^*\Big(t - \frac{\tau}{2}\Big)\, e^{-j2\pi f\tau}\, d\tau \, .$$

The WD provides high TF localization, in addition to satisfying many other important signal properties. However, it suffers from cross or inteference terms when analyzing multicomponent signals due to its quadratic nature. The cross terms can be misinterpreted as additional signal components to an untrained signal analyst, and thus the WD can lead to incorrect information. Various windowing or smoothing

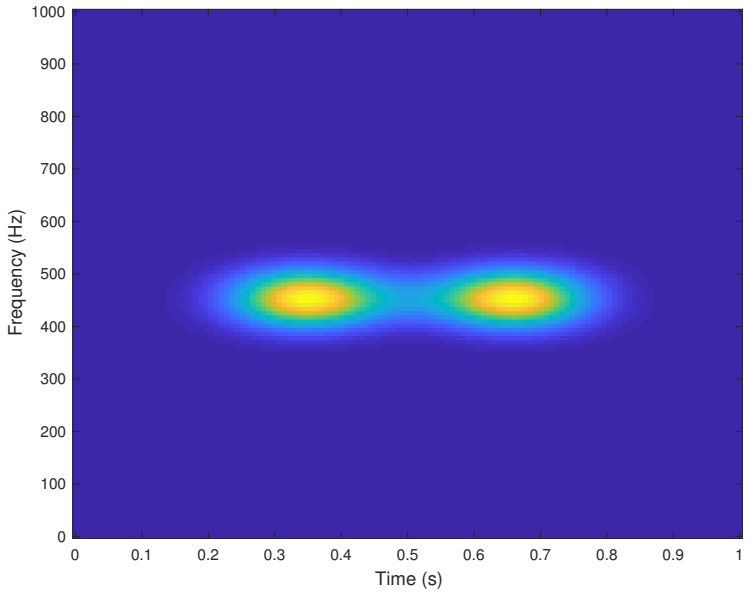

(a) Gaussian window with short duration

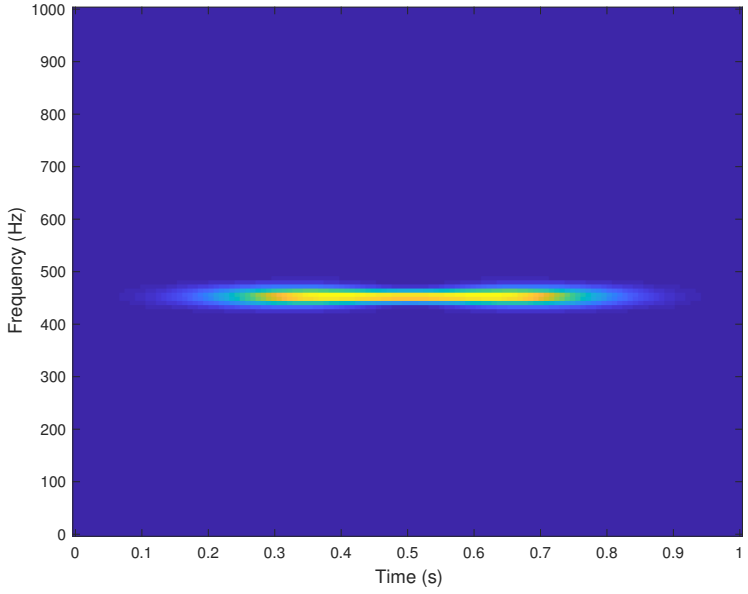

(b) Gaussian window with long duration

Figure 2.1: Spectrogram of a signal consisting of the sum of two Gaussian signals with varying duration T_g: (a) 0.13 s; (b) 0.5 s.

versions of the WD have been introduced to suppress cross terms; these however lead to TF resolution trade-off issues similar to those faced by the spectrogram [15]

In Figure 2.2(a), the WD is used to analyze two linear frequency-modulated (LFM) signals. These correspond to waveforms whose frequency content changes linearly with time. As shown in the figure, the WD perfectly localizes the two LFM signals in the TF plane as they appear as lines whose slope corresponds to the frequency modulation (FM) rate of each signal. Note that in this example, the FM rates of the signals were selected to be the same, thus the WD TFRs form parallel lines. Although TF localization is not a problem with the WD, the figure shows a third linearly-varying term in the middle of the two auto terms; this term corresponds to the undesirable cross-term between the two LFM signal components.

2.2 Reassignment Method

The reassignment method provides TFRs that are both highly localized in time and frequency and that do not suffer from cross terms [18–20]. The reassignment method was initially used with the spectrogram in [18] and then generalized to other TFRs in [19, 20]. When computing the spectrogram or other smoothed WDs, windowing results in the attenuation of cross terms while simultaneously causes spreading in time and frequency; this spreading results in a loss of TF resolution. In order to keep the reduction of cross terms but remove the TF spreading, the reassignment method is designed to move the TF center point of the averaging caused by a smoothed TFR to a new point that corresponds to the TF center of gravity of that representation. This TF shift to the center of gravity highly improves the readability of the resulting reassigned TFR.

The reassigned spectrogram of a signal $x(t)$, $t \in \mathcal{R}$, using an analysis window $g(t)$, can be obtained as follows: (a) the spectrogram of the signal is first computed with

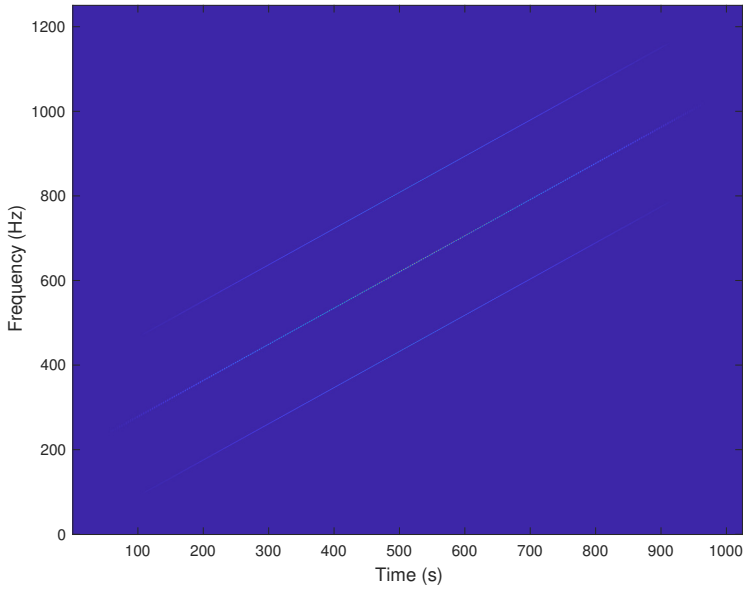

(a)

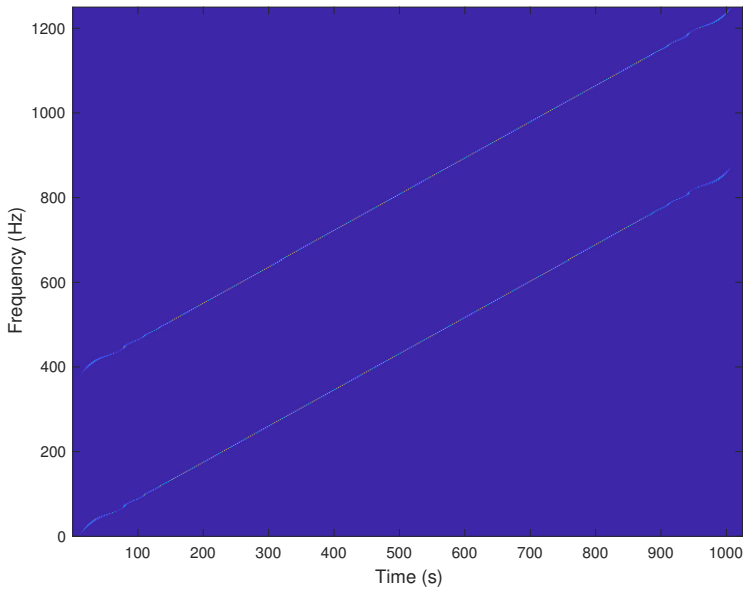

(b)

Figure 2.2: TFRs of a signal consisting of the sum of two LFM waveforms: (a) Wigner distribution; (b) Reassigned spectrogram.

the given window; (b) the TF coordinate of the center of gravity of the spectrogram is computed; and (c) the spectrogram is shifted in time and frequency to this new TF coordinate. Specifically, the reassigned spectrogram is defined as

$$R_x(t,f;g) = \int\int \mathrm{SP}_x(\tau,\nu;g)\,\delta\big(t-\eta_x(\tau,\nu)\big)\,\delta\big(f-\zeta_x(\tau,\nu)\big)\;\mathrm{d}\tau\,\mathrm{d}\nu$$

where $\mathrm{SP}_x(t,f;g)$ is the spectrogram of the signal and the TF coordinate of the center of gravity of the spectrogram can be obtained as

$$\begin{aligned}\eta_x(t,f) &= t - \frac{\int\int \tau\, W_g(\tau,\nu)\, W_x(t-\tau,f-\nu)\;\mathrm{d}\tau\,\mathrm{d}\nu}{\int\int W_g(\tau,\nu)\, W_x(t-\tau,f-\nu)\;\mathrm{d}\tau\,\mathrm{d}\nu}\\ \\ \zeta_x(t,f) &= f - \frac{\int\int \nu\, W_g(\tau,\nu)\, W_x(t-\tau,f-\nu)\;\mathrm{d}\tau\,\mathrm{d}\nu}{\int\int W_g(\tau,\nu)\, W_x(t-\tau,f-\nu)\;\mathrm{d}\tau\,\mathrm{d}\nu}\,,\end{aligned}$$

where $W_g(t,f)$ is the WD of the window $g(t)$. Note that $\eta_x(t,f)$ and $\zeta_x(t,f)$ are also called the time and frequency reassignment operators, respectively [19].

The reassignment operators can also be computed using the derivative of the phase function $\Phi_x(t,f;g)$ of the STFT. In particular, by first expressing the STFT in (2.1) in terms of its magnitude and phase,

$$S_x(t,f;g) = |S_x(t,f;g)|\, e^{j2\pi\Phi_x(t,f;g)}$$

then, it can be shown that [16]

$$\begin{aligned}\eta_x(t,f) &= -\frac{\partial}{\partial f}\,\Phi_x(t,f;g)\\ \\ \zeta_x(t,f) &= f + \frac{\partial}{\partial t}\,\Phi_x(t,f;g)\,.\end{aligned} \tag{2.2}$$

Efficient methods were developed in [19, 20] to compute the derivatives of the phase function of the STFT for use in real applications. Specifically, it can be shown that

$$\frac{\partial}{\partial t}\,\Phi_x(t,f;g) = -\mathrm{Im}\left(\frac{S_x(t,f;g_d)}{S_x(t,f;g)}\right)$$

where $g_d(t) = \dfrac{d}{dt} g(t)$ is the derivative of the window $g(t)$ and $\mathrm{Im}(\cdot)$ denotes the imaginary part, and

$$\frac{\partial}{\partial f}\,\Phi_x(t,f;g) = -t + \mathrm{Re}\left(\frac{S_x(t,f;g_t)}{S_x(t,f;g)}\right)$$

where $g_t(t) = t\,g(t)$ and $\mathrm{Re}(\cdot)$ denotes the real part. The resulting reassignment operators are thus given by

$$\eta_x(t,f) \;=\; t - \mathrm{Re}\left(\frac{S_x(t,f;g_t)}{S_x(t,f;g)}\right) \tag{2.3}$$

$$\zeta_x(t,f) \;=\; f + \mathrm{Im}\left(\frac{S_x(t,f;g_d)}{S_x(t,f;g)}\right). \tag{2.4}$$

Figure 2.2(b) shows the reassigned spectrogram of the two LFM waveforms that were analyzed by the WD in Figure 2.2(a). As it can be seen, the reassigned spectrogram preserved the high localization of the WD without the presence of the cross terms. Note than an adjustable version of reassignment was introduced in [21], where the extent of TF localization can be controlled. Also, in order to facilitate the real time implementation of the reassignment method, causal recursive filters were used in [22].

2.3 Synchrosqueezing Transform

2.3.1 Synchrosqueezing Transform TFR

Although the reassignment method provides highly localized TFRs, it cannot easily reconstruct the original signal [23]. The synchrosqueezing transform (SST), on the other hand, can operate directly on the STFT to obtain the same high TF resolution properties as the reassignment method and can also reconstruct the original signal. The SST reassigns the value of the STFT only along the frequency axis.

Specifically, the SST of a signal $x(t)$, $t \in \mathcal{R}$, is defined as

$$\mathrm{SST}_x(t, f; g) = \int S_x(t, \nu; g)\, \delta(f - \zeta_x(t, \nu))\, e^{j2\pi t f} d\nu\,, \tag{2.5}$$

where $S_x(t, f; g)$ is the STFT of the signal with window $g(t)$, and $\zeta_x(t, f)$ is the frequency reassignment operator in Equation (2.4). Figure 2.3(a) shows the SST TFR of a multicomponent signal consisting of one LFM waveform and one constant frequency waveform. In this example, the available bandwidth is 1.25 kHz and the waveform duration is 1 second. The sampling frequency used is $f_s = 2.5$ kHz. As it can be seen, the SST results in a highly localized TFR of the two signal components without any cross terms.

2.3.2 SST Ridge Extraction

The SST signal reconstruction is achieved by estimating the IF or ridge of each signal component. Specifically, the SST extracts the ridge of each signal component and then reconstructs each component by integrating the SST TFR in the vicinity of its corresponding ridge.

We assume that a multicomponent signal $x(t) = \sum_{k=1}^{K} x_k(t)$ is a linear combination of K components or modes. The kth mode is given by $x_k(t) = A_k(t)\, e^{j2\pi\, \phi_k(t)}$, with magnitude $A_k(t) > 0$ and phase function $\phi_k(t)$. An ideal representation of the multicomponent signal would be one that is highly localized in TF and does not suffer from cross terms. Such a TFR would consist of a linear combination of K instantaneous frequencies (IFs); the kth IF corresponds to the first derivative of the kth phase function $\phi'_k(t)$. Specifically, the ideal TFR of $x(t)$ is

$$\mathrm{ITFR}_x(t, f) = \sum_{k=1}^{K} A_k(t)\, \delta\big(f - \phi'_k(t)\big)\,. \tag{2.6}$$

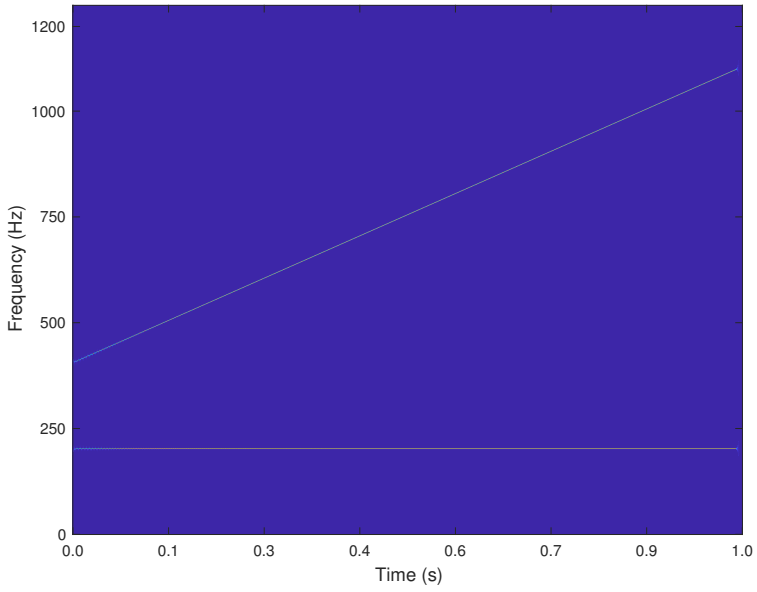

(a)

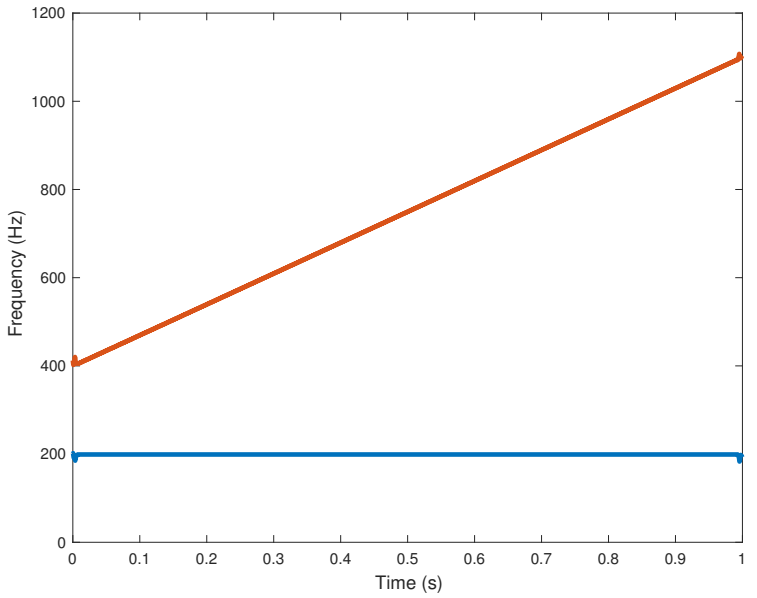

(b)

Figure 2.3: TFRs of a signal consisting of the sum of an LFM waveform and a constant frequency waveform: (a) SST; and (b) SST estimated IF.

An ideal TFR assumes that the energy of each mode is concentrated along its corresponding ridge. As a result, a ridge extracted from a highly localized TFR could be used to reconstruct its matched signal mode. Once all the ridges are extracted, each mode can be reconstructed by inverting the TFR around the vicinity of its corresponding ridge. The kth reconstructed signal mode is given by

$$\hat{x}_k(t) \approx \int_{\{f,|f-\phi_k'(t)|<d\}} \mathrm{SST}_x(t,f;g)\,df \tag{2.7}$$

for some small parameter d.

If the number of mode components K is assumed known and the SST $\mathrm{SST}_x(t,f;g)$ is given, then a ridge or IF estimation method can be used to estimate $\phi_k'(t)$ in (2.7) before the mode retrieval. One such method is based on minimizing the energy functional [24, 25]

$$E_x = \sum_{k=1}^{K}\left(-\int \left|\mathrm{SST}_x(t,\psi_k(t);g)\right|^2 dt + \int \left(\lambda\,\psi_k'(t)^2 + \beta\,\psi_k''(t)^2\right)dt \right). \tag{2.8}$$

This is achieved by solving for smooth functions $\psi_k(t)$ along which the magnitude of the SST is maximum. The constants λ and β are optimization control parameters that are used to trade off between function smoothness and energy maximization [25]. The minimization of (2.8) is approximated using methods such as simulated annealing and the crazy climbers algorithm [24–26]. Simulated annealing performs particularly well for finding a global maximum. However, to find the ridges, an algorithm that is more suited towards finding local maxima and minima is required. The crazy climbers algorithm initializes random points or climbers on the TF grid; the points then evolve based on the local values of the magnitude of the TFR. Following [25], we use an adaptation of the crazy climbers algorithm, described in Algorithm 1 [9]. Figure 2.3(b) shows the ridges extracted from the SST in Figure 2.3(a) using the crazy climbers algorithm. In Figure 2.4(a), the components are reconstructed using the estimated ridges and then compared to the original signal.

Algorithm 1 Crazy Climbers Algorithm [9, 25]

Obtain SST TFR, $\mathrm{SST}_x(t, f; g)$, $t \in (0, N)$ and $f \in (0, B)$

Divide TF plane into a grid $\mathcal{T} = \{0, 1, \ldots, N\} \times \{0, 1, \ldots, B\}$

Assign probability of moving forward or backward along time axis to be $p = 0.5$

Assign an integer value to M

Initialize a climber at TF point $(t_0, f_0) = \underset{t \in (0,N),\ f \in (0,B)}{\arg\max} \left|\mathrm{SST}_x(t, f; g)\right|$

for $t_n \leftarrow t_0$ to N **do**

Jump allowed in frequency at the next time step t_n: $f_n = [-M + f_{n-1}, M + f_{n-1}]$

Find next frequency bin f_n at time t_n by: $\underset{(t_n, f_n \in [-M+f_{n-1}, M+f_{n-1}])}{\arg\max} \left|\mathrm{SST}_x(t, f; g)\right|$

if $|\ \mathrm{SST}_x(t_n, f_n; g)\ | > \gamma$ **then**

Move climber to TF point (t_n, f_n)

else

End the movement of the climber at point (t_{n-1}, f_{n-1})

end if

end for

for $t_n \leftarrow t_0$ to 0 **do**

Jump allowed in frequency in next time step t_n: $f_n = [-M + f_{n-1}, M + f_{n-1}]$

Find next frequency bin f_n at time t_n by: $\underset{(t_n, f_n \in [-M+f_{n-1}, M+f_{n-1}])}{\arg\max} \left|\mathrm{SST}_x(t, f; g)\right|$

if $|\ \mathrm{SST}_x(t_n, f_n; g)\ | > \gamma$ **then**

Move climber to TF point (t_n, f_n)

else

End the movement of the climber at point (t_{n-1}, f_{n-1})

end if

end for

Zero out the region around the extracted ridge in $\mathrm{SST}_x(t, f; g)$.

Perform ridge extraction for remaining components in TF plane.

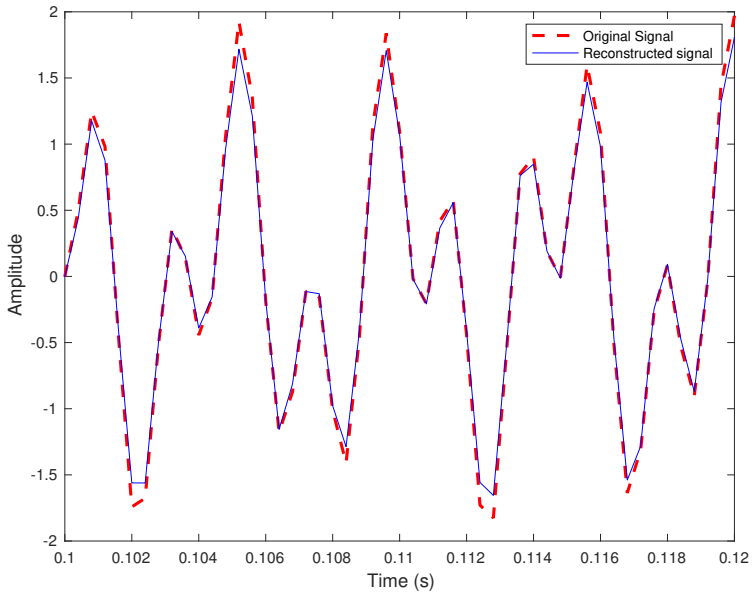

(a)

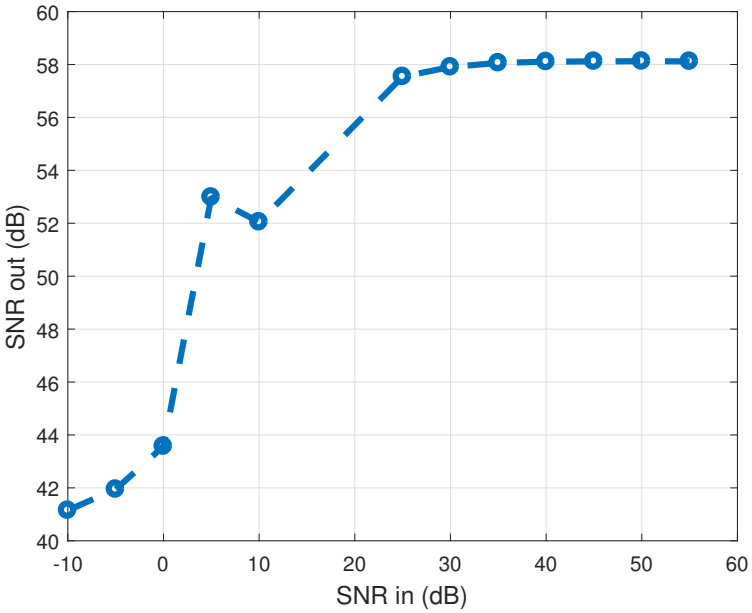

(b)

Figure 2.4: (a) Reconstructed waveform (from Figure 2.3) using SST estimated ridges with $d = 4$. (b) SST denoising performance: output vs input SNR of a signal in AWGN noise when analyzed using the SST.

2.3.3 Assumptions for SST Mode Reconstruction

The SST mode reconstruction is not valid for all signals. In particular, some assumptions must hold on the phase functions of the multicomponent signal modes. These assumptions were derived in [8] and summarized next.

(a) The signal modes must be well-separated in frequency; specifically, for a given Gaussian window $g(t;\sigma)$ with bandwidth $2\,B = \sqrt{2\log 2}/\sigma$, the following inequality must hold

$$\left|\phi_k'(t) - \phi_\ell'(t)\right| \geq 2\,B,\ \forall t,\ k,\ell = 1,\ldots,K,\ k \neq \ell$$

where $\phi_k'(t)$, the first derivative of the phase function $\phi_k(t)$, is the IF of the kth signal mode.

(b) All signal modes must have weak frequency modulation; specifically, assuming small $\epsilon > 0$, the following must hold

$$\sigma^2\left|\phi_k''(t)\right| \leq 2\,\epsilon \ \text{ and } \ \left|A_k'(t)\right| \leq \epsilon\,\phi_k'(t)\,,\ \forall t,\ k = 1,\ldots,K$$

where $\phi_k''(t)$ is the second derivative of the phase function $\phi_k(t)$

2.3.4 Denoising Performance

As the SST provides highly accurate estimates of the IF of a signal, under the aforementioned assumptions, it can be used as a tool for signal denoising. It was shown in [23] that the SST exhibits a better denoising performance than block thresholding techniques. As this advantage of the SST is important in all real applications we demonstrate the its denoising performance with an example. We consider a linear FM signal in additive white Gaussian noise (AWGN) and vary the signal-to-noise ratio (SNR) (or SNR_{in}). The SST based denoising simply estimates the ridges and reconstructs the signal as in (2.7). The output SNR is obtained using the reconstructed

signal as

$$\mathrm{SNR}_{\mathrm{out}} = \frac{\int x^2(t)\,dt}{\int \Big(x(t) - \hat{x}(t)\Big)^2\,dt}\,.$$

Figure 2.4(b) shows the output SNR for varying input SNR values. As it can be seen, the SST denoising performance increases with increasing input SNR.

Chapter 3

LINEAR INSTANTANEOUS FREQUENCY ESTIMATION

3.1 Biased Estimator for Linear Instantaneous Frequency

The synchrosqueezing transform (SST) discussed in Section 2.3 is defined in (2.5) using the frequency reassignment operator $\zeta_x(t, f)$. Following this definition, the usefulness of the SST for signal reconstruction depends on the accuracy with which the SST can estimate the instantaneous frequency (IF) of each signal component. As discussed in Section 2.3.3, one of the assumptions needed for mode reconstruction is that all modes are required to have weak frequency modulation. When this assumption does not hold, then the reconstruction is not accurate as it can be shown that the resulting IF estimate (IFE) obtained using the SST is biased. This is demonstrated next using a signal with a high frequency modulation.

We consider a linear frequency-modulated (LFM) signal given by

$$x(t) = A(t)\, e^{j2\pi\,\phi(t)} = A(t)\, e^{j2\pi\, c\, t^2}$$

where $c \in \mathcal{R}$ is the frequency modulation (FM) rate of the signal. We assume that the amplitude modulation $A(t) = A\, e^{(t-\mu)^2/(2\,\sigma^2)}$, $A > 0$, is a Gaussian function. An unbiased estimate of the LFM is given by the first derivative of the phase function $\phi(t) = c\, t^2$, given by $\phi'(t) = 2\, c\, t$. The IFE based on the SST is given by the frequency reassignment operator $\zeta_x(t, f)$ in Equation (2.4).

To obtain the SST IFE, we take the first derivative of the signal $x(t)$, as that is the step used to obtain Equation (2.2). The derivative of $x(t)$ can be written as

$$\frac{\partial}{\partial t} x(t) = \left(\frac{\partial}{\partial t} A(t) + j2\pi\, \frac{\partial}{\partial t}\, \phi(t) \right) x(t) = (a_x\, t + b_x)\, x(t) \tag{3.1}$$

where $a_x = -1/\sigma^2 + j2\pi(2\,c)$ and $b_x = \mu/\sigma^2$. Note that the imaginary part of the term $a_x\,t + b_x = -(t-\mu)/\sigma^2 + j2\pi(2\,c\,t)$ is the IF of $x(t)$. From (2.2), the IFE estimate can be written as $\zeta_x(t,f) = f + \dfrac{\partial}{\partial t}\,\Phi_x(t,f;g)$, where $\Phi_x(t,f;g)$ is the phase function of the short-time Fourier transform (STFT) of the signal, $S_x(t,f;g) = |S_x(t,f;g)|\,e^{j2\pi\,\Phi_x(t,f;g)}$, with analysis window $g(t)$. Taking the derivative of the STFT results in

$$\frac{\partial}{\partial t} S_x(t,f;g) = S_x(t,f;g_d) = -a_x\,S_x(t,f;g_m) + (a_x\,t + b_x - j2\pi f)\,S_x(t,f;g), \quad (3.2)$$

where $g_d(t) = \frac{d}{dt}g(t)$, $g_m(t) = t\,g(t)$, and $S_x(t,f;g_d)$ and $S_x(t,f;g_m)$ are the STFTs of $x(t)$ with windows $g_d(t)$ and $g_m(t)$, respectively. Dividing Equation (3.2) with $S_x(t,f;g)$, and rearranging the terms, results in

$$j2\pi\,f + \frac{S_x(t,f;g_d)}{S_x(t,f;g)} = a_x\left(t - \frac{S_x(t,f;g_m)}{S_x(t,f;g)}\right) + b_x\,. \quad (3.3)$$

From (3.1), the imaginary part of $a_x t + b_x$ is the IF of the LFM. So, taking the imaginary part of Equation (3.3), and using the definition of the reassignment operators in Equations (2.3) and (2.4), results in the SST IFE as

$$\hat{\zeta}_x(t,f) = 2\,c\,\hat{\eta}_x(t,f)\,. \quad (3.4)$$

As it can be seen from Equation (3.4), the estimated IF $\hat{\zeta}_x(t,f)$ is biased since it is calculated at time $\hat{\eta}_x(t,f)$ instead of at time t.

This is also evident from the fact that the second assumption in Section 2.3.3, given by $\sigma^2\left|\phi_k''(t)\right| \le 2\,\epsilon$, for small $\epsilon > 0$ and using a Gaussian window $g(t)$ with parameter σ^2, does not hold for large FM rates c. Specifically, $\phi''(t)^2 = 4c^2$, and for large values of c, $4\sigma^2\,c^2 > 2\,\epsilon$.

3.2 Unbiased Linear Instantaneous Frequency Estimation

In [27], a second order SST was introduced that is matched to signals with higher frequency modulation. It was then used in [13] to derive unbiased IF estimates for

LFM signals. We consider the LFM signal from Section 3.1, $x(t) = A(t)\, e^{j2\pi ct^2}$, where $A(t) = A\, e^{(t-\mu)^2/2\sigma^2}$. If we differentiate Equation (3.2) with respect to time, we obtain

$$S_x(t, f; g_{dd}) = -a_x\, S(t, f; g_{md}) + (a_x\, t + b_x - j2\pi f)\, S_x(t, f; g_d) \tag{3.5}$$

where $S_x(t, f; g_{md})$ and $S_x(t, f; g_{dd})$ are the STFTs of $x(t)$ computed using analysis windows $g_{md}(t) = t\dfrac{d}{dt}g(t)$ and $g_{dd}(t) = \dfrac{d^2}{dt^2}g(t)$, respectively. Equations (3.2) and (3.5) form a system of two linear equations with variables a_x and $(a_x\, t + b_x - j2\pi f)$. Solving the system of linear equations and taking the imaginary part of $(a_x\, t + b_x - j2\pi f)$ provides an unbiased IFE that is given by

$$\hat{\zeta}_x^{(2)}(t, f) = f + \mathrm{Im}\left(\frac{S_x(t, f; g_{dd})\, S_x(t, f; g_m) - S_x(t, f; g_{md})\, S_x(t, f; g_d)}{S_x(t, f; g_d)\, S_x(t, f; g_m) - S_x(t, f; g_{md})\, S_x(t, f; g)} \right), \tag{3.6}$$

where $\mathrm{Im}(\cdot)$ represents the imaginary part. The IFE in Equation (3.6) is known as the second order synchrosqueezing operator and it is discussed in detail in [28].

In general, higher orders of unbiased IFEs can also be derived by taking higher order derivatives, order $n \geq 2$, of Equation (3.5). This results in

$$\begin{aligned} \frac{\partial^n}{\partial t^n}\, S_x(t, f; g) &= S_x(t, f; g_{d,n}) \\ &= -a_x\, S_x(t, f; g_{md,n-1}) + (a_x\, t + b_x - j2\pi f)\, S_x(t, f; g_{d,n-1}), \end{aligned} \tag{3.7}$$

where $g_{d,n}(t) = \dfrac{\partial^n}{\partial t^n}\, g(t)$, $g_{d,n-1}(t) = \dfrac{\partial^{n-1}}{\partial t^{n-1}}\, g(t)$, and $g_{md,n-1}(t) = t\, \dfrac{\partial^{n-1}}{\partial t^{n-1}}\, g(t)$. Solving Equations (3.2) and (3.7) results in the nth order unbiased IFE given by

$$\hat{\zeta}_x^{(n)}(t, f) = f + \mathrm{Im}\left(\frac{S_x(t, f; g_{d,n})\, S_x(t, f; g_m) - S_x(t, f; g_{md,n-1})\, S_x(t, f; g_d)}{S_x(t, f; g_{d,n-1})\, S_x(t, f; g_m) - S_x(t, f; g_{md,n-1})\, S_x(t, f; g)} \right). \tag{3.8}$$

If the signal $x(t)$ has constant amplitude modulation, then the corresponding unbiased IFE in (3.6) can be shown to be [13]

$$\hat{\zeta}_x^{(2)M}(t, f) = f - \frac{\mathrm{Re}(S_x(t, f; g_d)\, S_x^*(t, f; g_m))}{\mathrm{Im}(S_x(t, f; g)\, S_x^*(t, f; g_m))}. \tag{3.9}$$

Similarly, the corresponding nth order unbiased IFE in (3.8) for an LFM with no amplitude modulated can be shown to be

$$\hat{\zeta}_x^{(n)M}(t,f;n) = f - \frac{\mathrm{Re}\Big(S_x(t,f;g_{d,n})\, S_x^*(t,f;g_{md,n-1})\Big)}{\mathrm{Im}\Big(S_x(t,f;g_{d,n-1})\, S_x^*(t,f;g_{md,n-1})\Big)} \tag{3.10}$$

$$\tag{3.11}$$

3.3 Modified Synchrosqueezing Transform

The unbiased IFEs in the previous section, derived for either Gaussian amplitude modulated or constant amplitude LFM signals, can be used to modify the SST. The resulting highly localized modified synchrosqueezing transforms (MSST) that are matched to LFM signals and provide unbiased IFEs when the signals have high frequency modulation. The MSST can be given by

$$\mathrm{MSST}_x(t,f;g) = \int_\nu S_x(t,\nu;g)\ \delta(f - r_x(t,\nu))\, e^{j2\pi ft}\, d\nu \tag{3.12}$$

where $r_x(t,\nu) = \hat{\zeta}_x^{(2)}(t,f)$ in Equation (3.6) or $r_x(t,\nu) = \hat{\zeta}_x^{(n)}(t,f)$ in Equation (3.8) for Gaussian amplitude modulated LFM signals. For constant amplitude LFM signals, $r_x(t,\nu) = \hat{\zeta}_x^{(2)M}(t,f)$ in Equation (3.9) or $r_x(t,\nu) = \hat{\zeta}_x^{(n)M}(t,f)$ in Equation (3.10).

In Figure 3.1(a), the MSST of an LFM signal with no amplitude modulation and 25 dB SNR is shown. Figure 3.1(b) shows the MSST of an LFM signal with Gaussian amplitude modulation and 25 dB SNR. The available bandwidth is 40 MHz and the signal duration is 20 μs. The sampling frequency used is 100 MHz. Figure 3.2 demonstrates the reconstruction performance of the biased SST and the unbiased MSST with the $\hat{\zeta}_x^{(2)}(t,f)$ IFE in (3.6). For this example, we used an LFM signal with Gaussian amplitude modulation, 1 kHz bandwidth, 1 s duration, and 2.5 kHz sampling frequency. The biased SST and unbiased MSST are shown in Figures 3.2(a) and 3.2(b), respectively. After ridge extraction, the component is reconstructed using

$d = 1$ in Equation (2.7). Figure 3.2(c) is the reconstructed signal from the biased SST and Figure 3.2(d) is the reconstructed signal from the unbiased MSST. As it can be observed, the unbiased MSST results in a more accurate reconstructed signal for the given value of d.

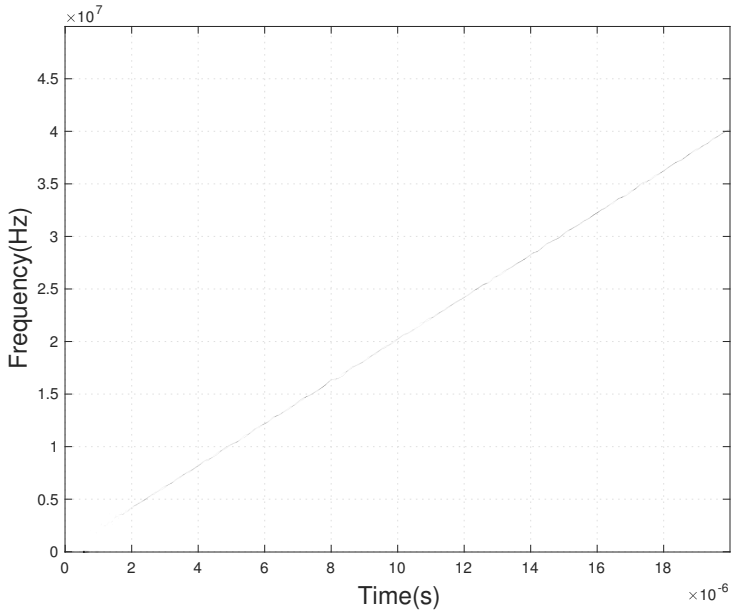

(a)

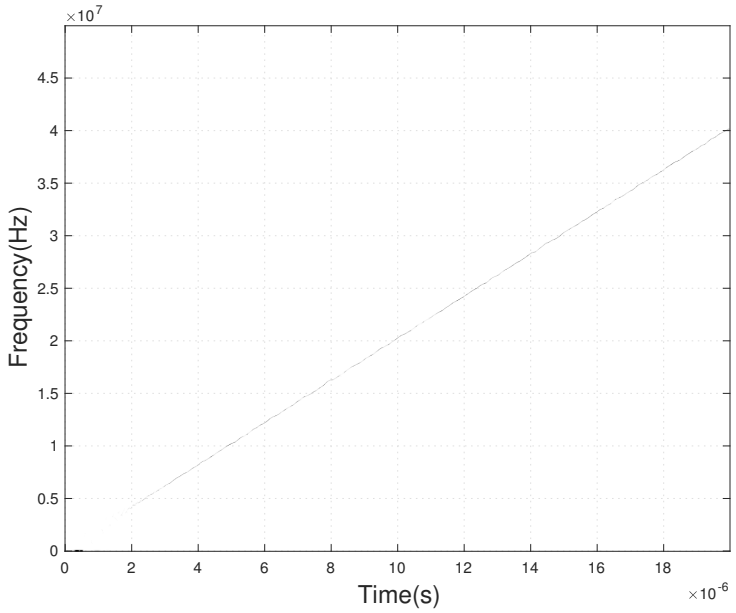

(b)

Figure 3.1: TFR analysis of high frequency modulated LFM signal in 25 dB SNR using MMST computed with (a) unbiased IFE $\phi_x^{K1}(t, f)$; and (b) unbiased IFE $\phi_x^{t2}(t, f)$.

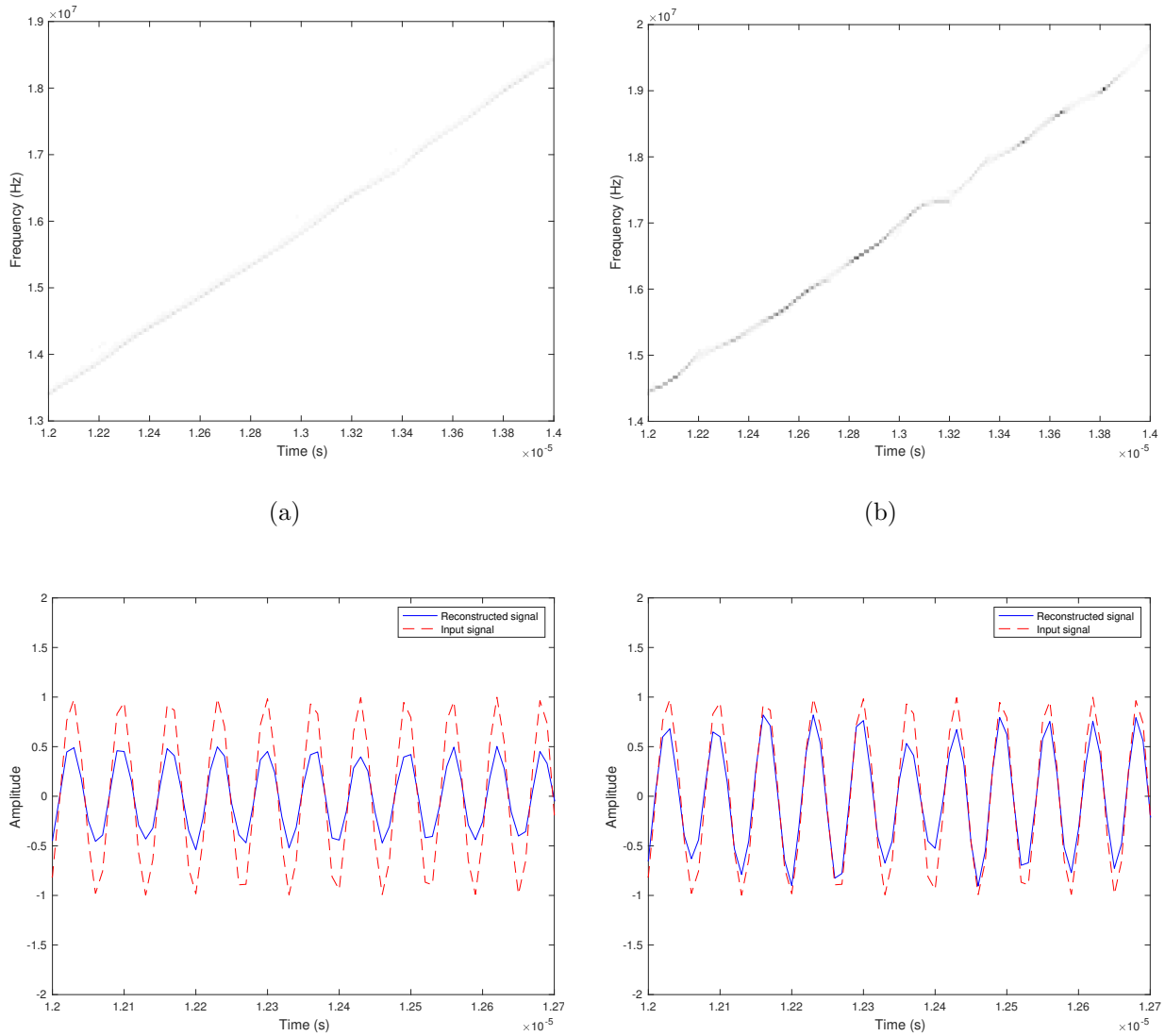

(a) (b)

(c) (d)

Figure 3.2: TFR analysis (zoomed in) of linear FM using (a) SST generated using $\hat{\zeta}_x(t,f)$ in (2.4) and (b) MSST generated using $\hat{\dot{\phi}}^{t2}(t,f)$ in (3.6). linear FM signal reconstruction using (c) biased SST and (d) unbiased MSST.

Chapter 4

NONLINEAR INSTANTANEOUS FREQUENCY ESTIMATION

4.1 Unbiased Nonlinear IF Estimation

The advantage of using highly nonlinear frequency-modulated (NFM) waveforms to increase the performance of multimodal coexisting systems has already been demonstrated [1, 4, 5, 29]. It is thus important to be able to design unbiased instantaneous frequency (IF) estimators for waveforms other than linear frequency-modulated (LFM) ones, as in Chapter 3. In this work, we propose the design of such unbiased NFM IF estimators that make use of the modified synchrosqueezing transform (MSST) discussed in Section 3.3 and warping axis tranformations [16, 30–34].

Consider a nonlinear FM waveform

$$x(t) = A\, e^{j2\pi\, c\, \phi_x(t)}$$

with constant amplitude $A > 0$, frequency modulation (FM) rate c, nonlinear time-varying phase function $\phi_x(t)$, and IF given by the derivative of the phase function, $\nu_x(t) = c\,\dfrac{d}{dt}\phi_x(t)$. The design steps for estimating the nonlinear IF involve of the NFM is to first warp the time axis of the NFM signal $x(t)$ to obtain an LFM signal $y(t)$; to use the already discussed methods in Chapter 3 for estimating the linear IF of the LFM; and to warp the axis of the linear IF to match the nonlinearity in the phase function of the original signal $x(t)$. Specifically, the following steps can be used to provide an unbiased modified synchrosqueezing transform (MSST) IFE for the NFM signal.

W1. Warp the time-axis of the nonlinear FM signal $x(t)$ using the warping operator $\mathcal{W}$ to obtain

$$y(t) = (\mathcal{W}x)(t) = x\Big(\phi_x^{-1}(t^2)\Big) = A\, e^{j2\pi c\, t^2}. \tag{4.1}$$

Assuming that $\phi_x(t)$ is an invertible function, then Equation (4.1) holds since it can be shown that $x\big(\phi_x^{-1}(t^2)\big) = A\, e^{j2\pi\, c\, \phi_x\left(\phi_x^{-1}(t^2)\right)} = A\, e^{j2\pi c\, t^2}$.

W2. Compute the MSST in Equation (3.12) with $r_x(t,\nu) = \hat{\zeta}_x^{(2)M}(t,f)$ in Equation (3.9) or $r_x(t,\nu) = \hat{\zeta}_x^{(n)M}(t,f)$ in Equation (3.10). Ridge extraction, as discussed in Section 2.3.2, can then be used on the MSST to obtain an unbiased estimate of the IF of $y(t)$ as $\hat{\nu_y}(t) \approx 2\, c\, t$. Note that the unbiased IFE provides an estimate of the unknown FM rate c.

W3. Warp the time axis of the IFE of $y(t)$ using

$$\hat{\nu_x}(t) = \hat{\nu_y}\left(\frac{1}{2}\frac{d}{dt}\phi_x(t)\right) \tag{4.2}$$

to obtain the unbiased estimate of the IF of $x(t)$. In particular, using the IF axis warping in (4.2), it can be shown

$$\hat{\nu_y}\left(\frac{1}{2}\frac{d}{dt}\phi_x(t)\right) = 2\, c\, \frac{1}{2}\frac{d}{dt}\phi_x(t) = c\, \frac{d}{dt}\phi_x(t) = \hat{\nu_x}(t)$$

For the above warping process to be possible, some conditions on the nonlinearity of the phase function $\phi_x(t)$ must be satisfied. In particular, the following conditions must hold.

C1. The inverse function $\phi_x^{-1}(t)$ of the phase function $\phi(t)$ must exist for $t \in \mathcal{R}^+$; that is, $\phi_x^{-1}(\phi_x(t)) = t$, $\forall t$.

C2. The function $\phi_x(t)$ must be a continuous differentiable function that satisfies $\phi'_x(t) = \dfrac{d}{dt}\phi_x(t) > 0$, $\forall t$.

C3. Given a maximum available bandwidth B, then the maximum frequency of the warped NFM signal, which is the resulting LFM signal $y(t)$ in (4.1), cannot exceed B. This can be ensured when the following condition is satisfied

$$\frac{2\,T_d}{\phi'_x(T_d)} \leq 1\,,$$

where T_d is the duration of both the LFM and NFM signals.

The warping steps W1-W3 are demonstrated in Figure 4.1 using a power FM signal, $x(t) = e^{j2\pi\,c\,t^3}$ of 20 μs duration, 40 MHz bandwidth, and 100 MHz sampling frequency; the FM rate used is $c = 3.33{\times}16$ Hz^3. After the power FM signal is warped in Step W1 using $\phi_x(t) = t^3$, the resulting signal $y(t)$ is an LFM; the IF of this signal is shown in Figure 4.1(a) to be linear, as expected after the warping. After Step W3, the time axis of the linear IF is warped to obtain the expected nonlinearity $\phi'_x(t) = 3\,t^2$, as demonstrated in Figure 4.1(b).

4.2 Simulation Examples of Linear and Nonlinear IF Estimation

We demonstrate the performance of the various biased and unbiased IF estimation methods for different linear and nonlinear FM signals, as discussed in Chapter 3 and in this chapter, using simulations. We also consider a realistic scenario of coexisting radar and communications systems with different IF signatures and varying signal-to-noise ratio (SNR) conditions.

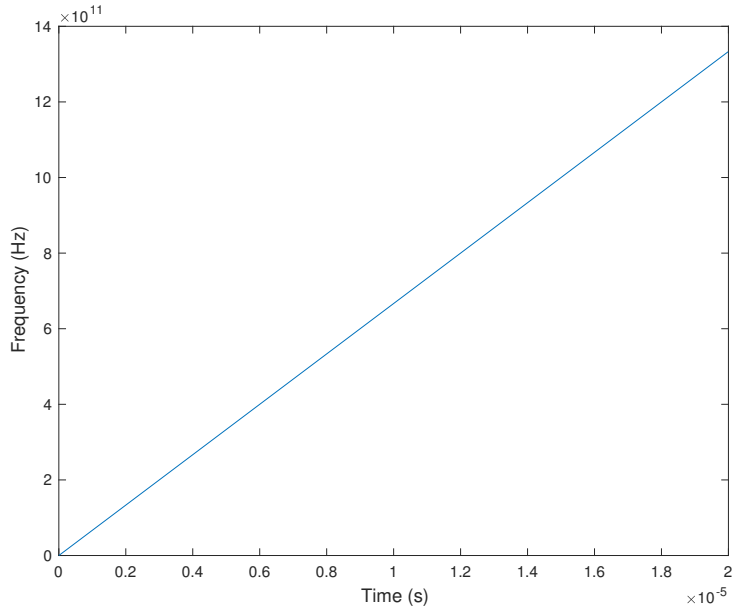

(a)

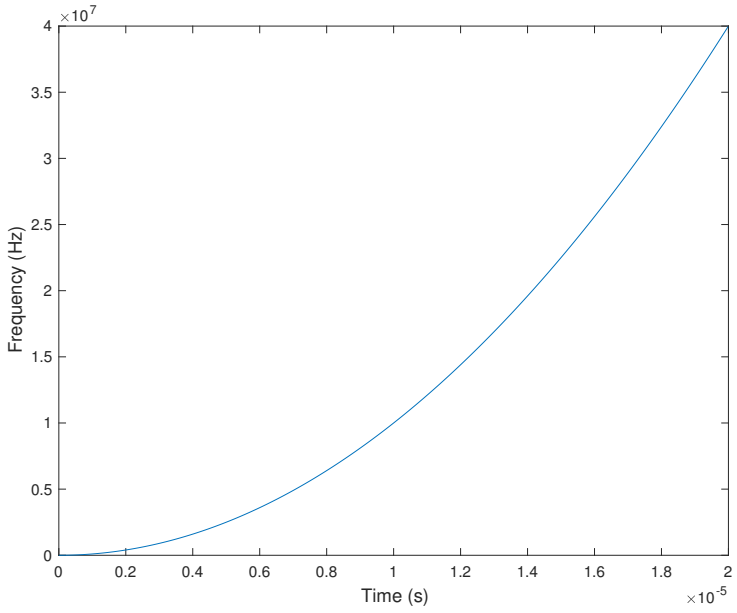

(b)

Figure 4.1: (a) IF of a warped power FM signal; (b) warped time axis of the IF of the signal in (a).

4.2.1 Linear Frequency-Modulated Waveforms

We consider an LFM signal of $T_d = 20$ μs duration, $B = 40$ MHz bandwidth and 100 MHz sampling frequency. The FM rate of the LFM signal $x(t) = e^{j2\pi c\, t^2}$ is $c = \frac{B}{2T_d}$. We consider two SNR values, 10 dB and 20 dB, and we run 40 Monte Carlo (MC) simulations. Figure 4.2(a) shows the biased SST IFE in (2.4) of the LFM in 20 dB SNR, whereas Figure 4.2(b) shows the unbiased MSST IFE in (3.6) of the same signal. Figures 4.3(a) and 4.3(b) show the corresponding ridges extracted for the biased SST and the unbiased MSST, respectively. As it can be seen, the biased SST in Figure 4.3(a) does not result in as accurate an IF estimate as the unbiased MSST one in Figure 4.3(b). In Figure 4.4, we compare the mean-squared error (MSE) between the estimated and actual IFs for 20 dB and 10 dB SNR for both the biased SST and unbiased MMST IFEs. The MSE for the unbiased MSST IFE is 20 dB lower when compared to the corresponding one for the biased SST IFE.

4.2.2 Power Frequency-Modulated Waveforms

We consider a power FM signal, $x(t) = e^{j2\pi c t^3}$, with $T_d = 20$ μs duration, $B = 40$ MHz bandwidth and 100 MHz sampling frequency. Figures 4.5(a) 4.5(b) show the SST and the MMST of the signal; the MMST is formed using (3.6) which is well-matched to LFM signals. Figures 4.6(a) and 4.6(b) show the estimated ridges obtained using the biased SST and unbiased MSST. The MSE obtained between the estimated and true IFs is shown in Figure 4.7(a). Note that, although both of these IFEs are matched to LFMs and not power FMs, the best performance is shown by the unbiased MSST at high SNR. At low SNR values, both IFEs do not perform well. Figure 4.7(b) compares the MSE of only the unbiased MSST but for both the LFM and the power FM signals for 20 dB and 10 dB SNR. Note that the best performance is achieved

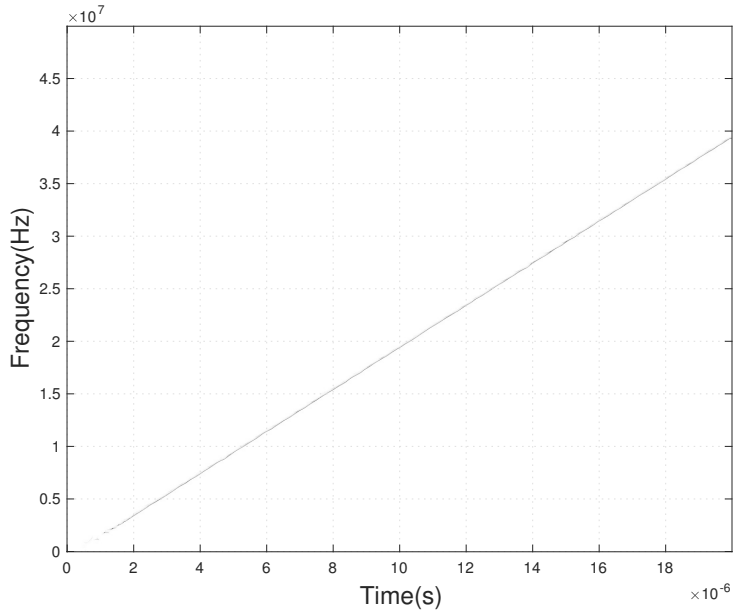

(a)

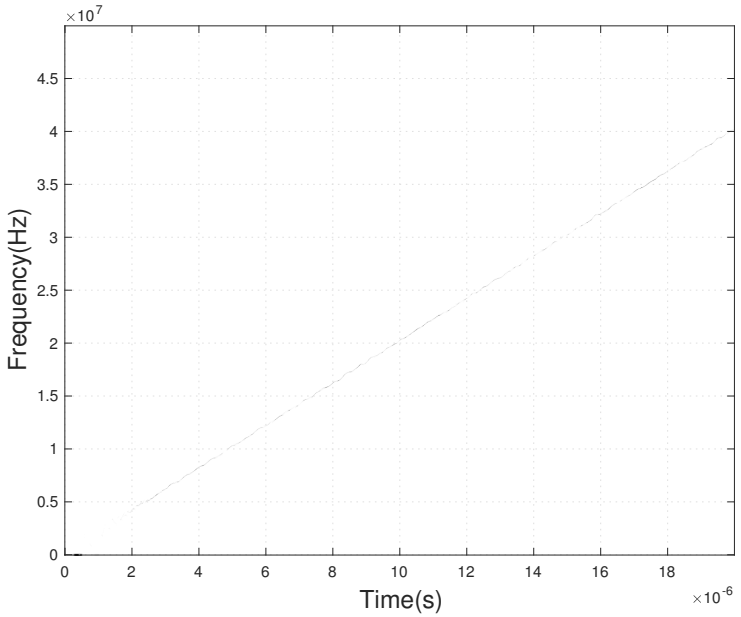

(b)

Figure 4.2: TFRs for LFM in 20 dB SNR: (a) SST using biased IFE in (2.4); (b) MSST using unbiased IFE in (3.6).

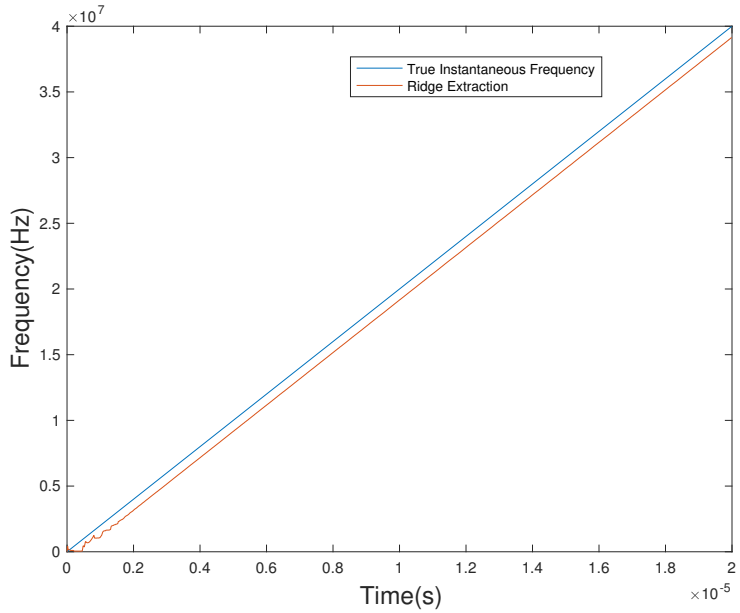

(a)

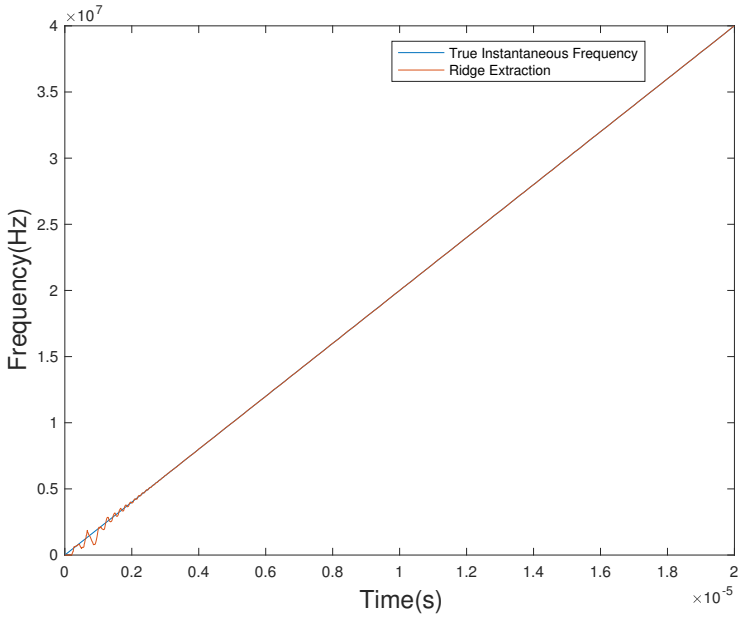

(b)

Figure 4.3: LFM signal ridges extracted from the: (a) unbiased SST in Figure 4.2(a) and (b) unbiased MSST in Figure 4.2(b).

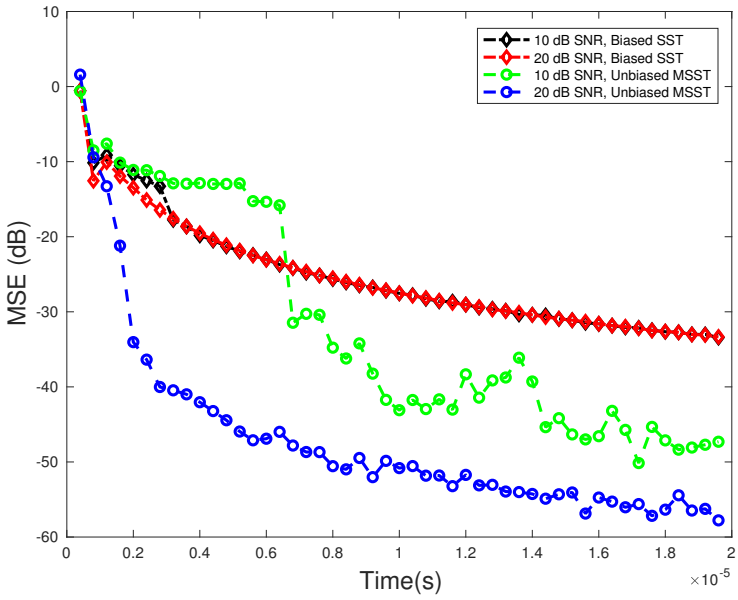

Figure 4.4: MSE of LFM estimated ridges using biased SST and unbiased MMST IFEs for 20 dB and 10 dB SNR.

by the unbiased MSST with the LFM signal at 20 dB SNR; this is expected as the unbiased MSST is designed to match LFM signals.

4.2.3 Signaling Scheme of Coexisting Scheme

We consider a realistic scenario of a coexisting multimodal system that includes a radar and a communications system, both at 20 dB SNR. The radar transmit waveform has nonlinear IF, given by $\nu_x(t) = 3\,c\,t^2$, and it is the signal of interest that needs to be extracted at the receiver. The communications system is designed to use LFM transmit signals; at the radar receiver, the LFM signals act as interference to the radar signal of interest. The signaling scheme is shown by the biased SST and unbiased MSST in Figures 4.8(a) and 4.8(b), respectively. Figures 4.9(a) and 4.9(b) show the ridges extracted using the biased SST and unbiased MSST. As it can be

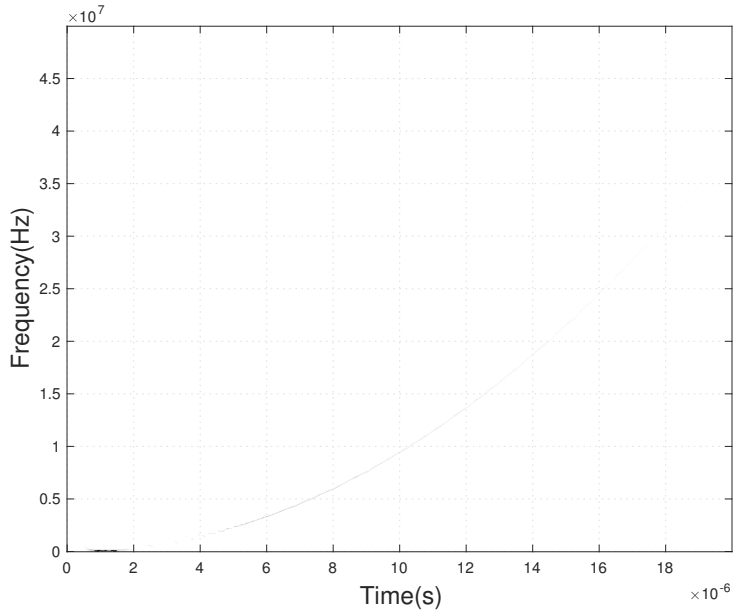

(a)

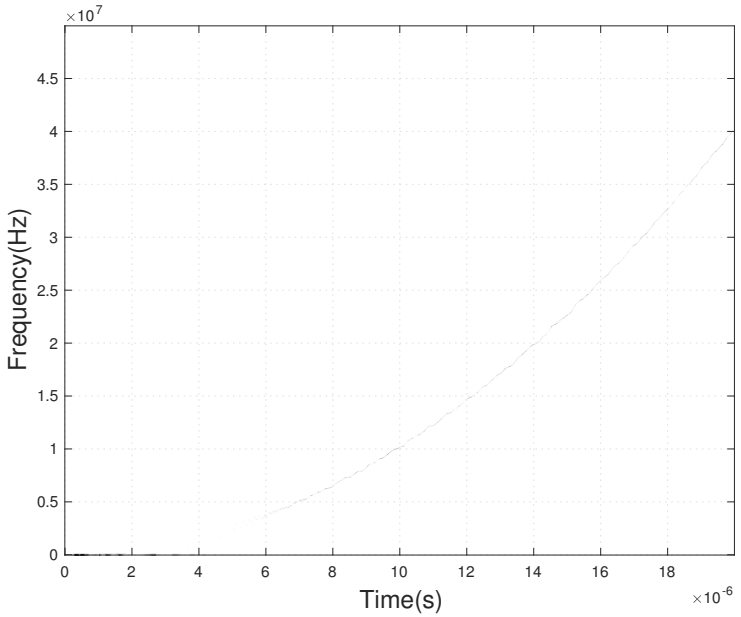

(b)

Figure 4.5: TFRs for power FM in 20 dB SNR: (a) SST using biased IFE in (2.4); (b) MSST using unbiased IFE in (3.6).

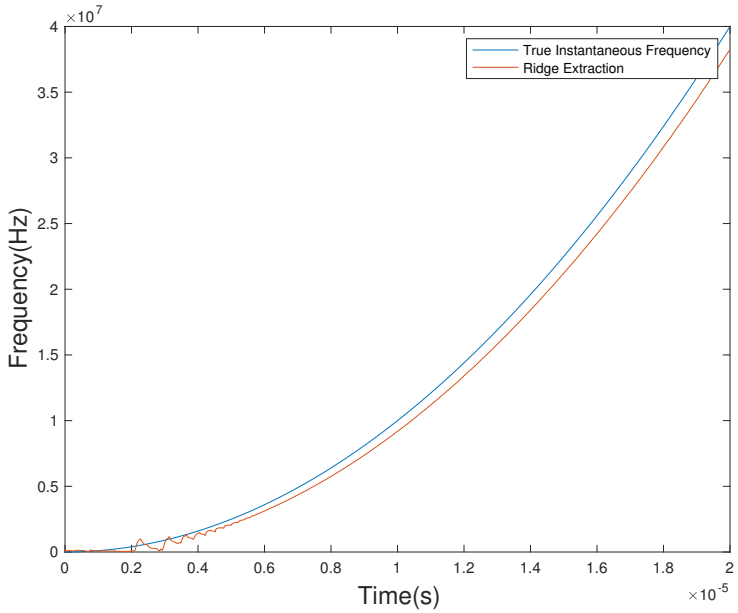

(a)

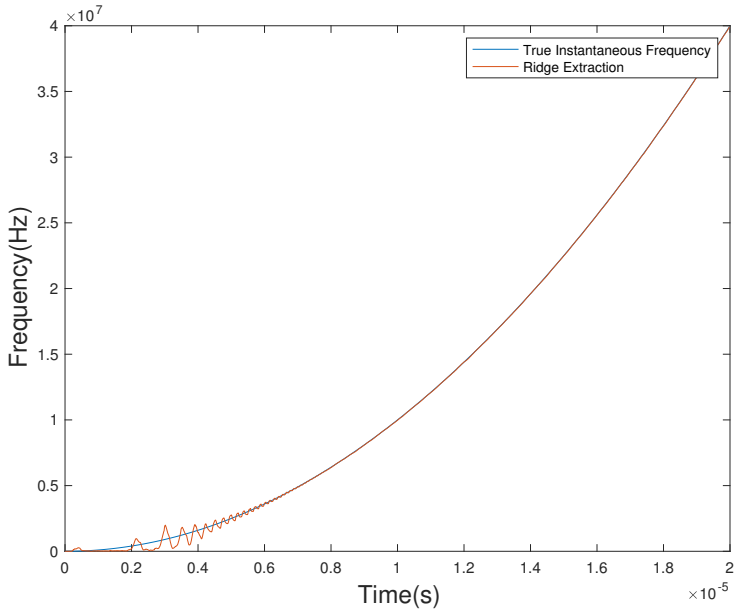

(b)

Figure 4.6: Power FM signal ridges extracted from the (a) biased SST in Figure 4.5(a) and (b) unbiased MSST in Figure 4.5(b).

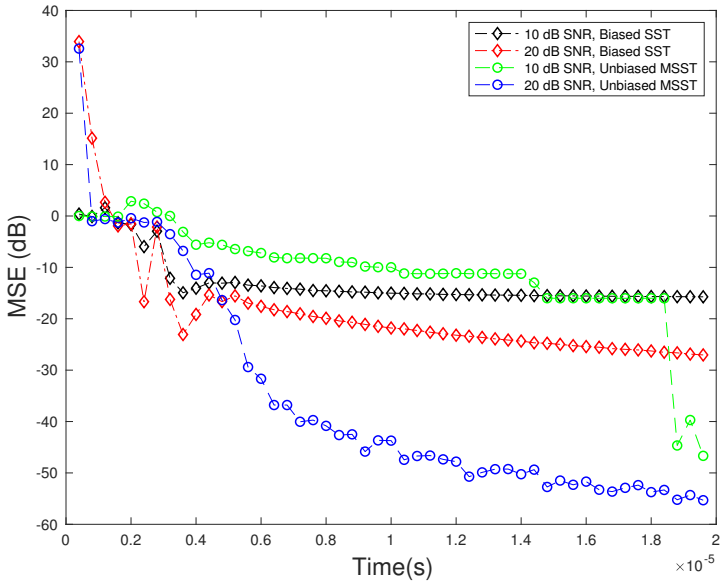

(a)

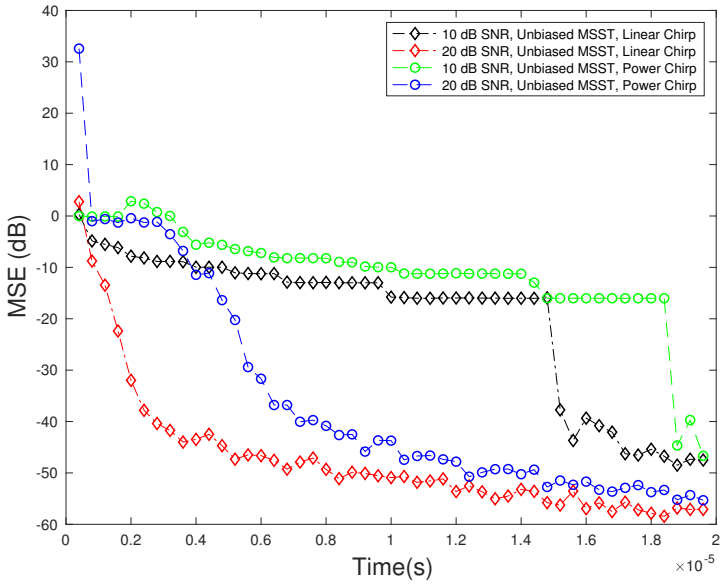

(b)

Figure 4.7: (a) MSE of power FM estimated ridges for 20 dB and 10 dB SNR using biased SST IFE and unbiased MMST IFE; (b) MSE of LFM and power FM estimated ridges for 20 dB and 10 dB SNR using unbiased MMST IFE.

seen, the MSST provides a better IF estimate; this estimate is then used to extract only the radar waveform, as shown in Figure 4.10.

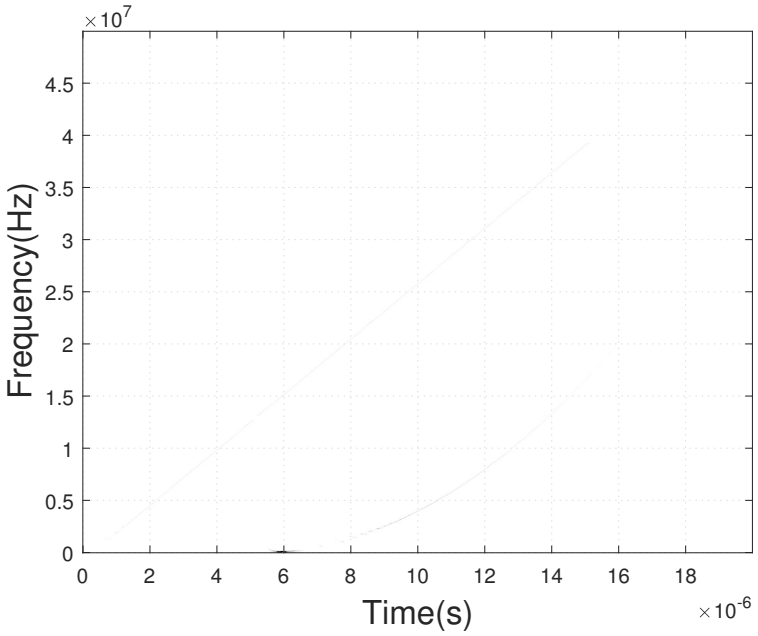

(a)

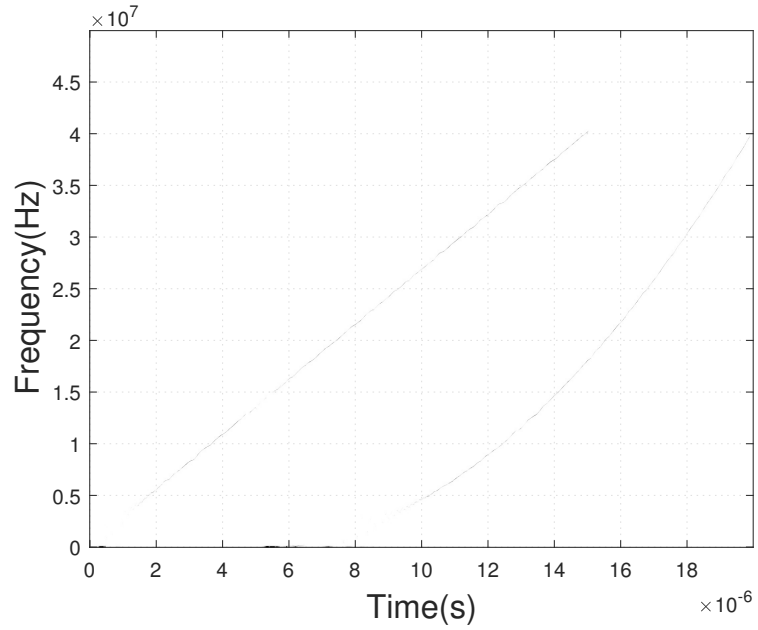

(b)

Figure 4.8: TFRs for the linear and power FM signals at 20 dB SNR in the multimodal system: (a) SST and (b) MSST.

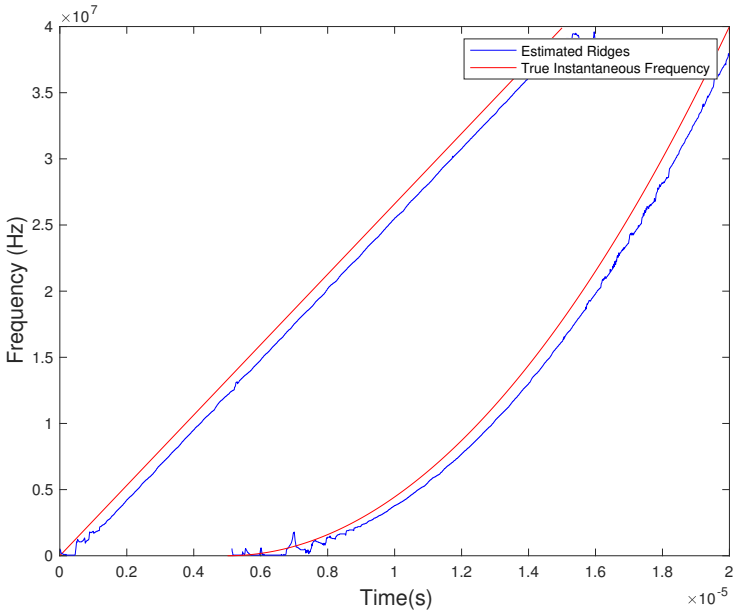

(a)

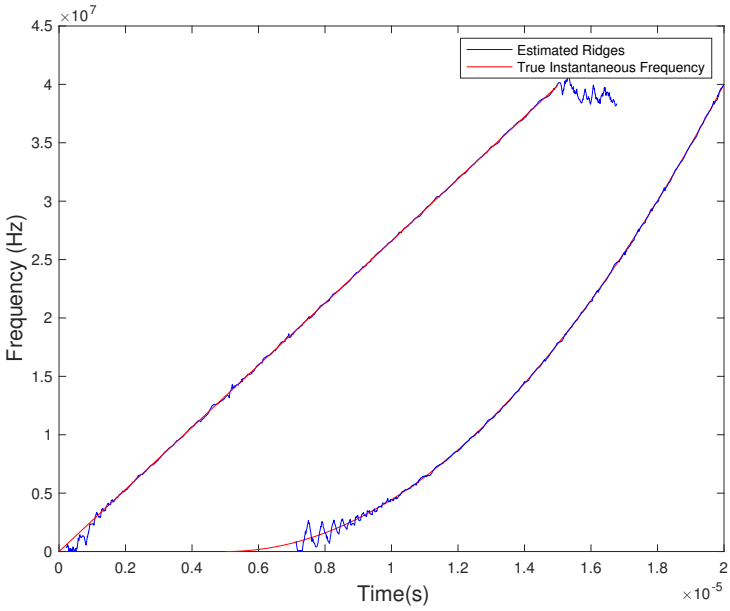

(b)

Figure 4.9: LFM and power FM signal ridges extracted from the (a) biased SST and (b) unbiased MSST.

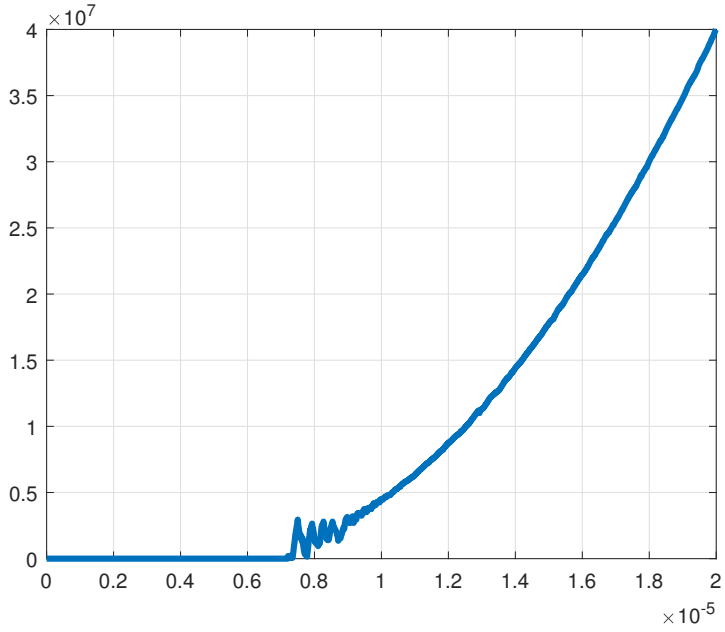

Figure 4.10: Extracted nonlinear IF of the signal matched to the radar receiver.

Chapter 5

CONCLUSIONS AND FUTURE WORK

5.1 Conclusions

This thesis demonstrates the use of highly localized time-frequency (TF) representation to resolve components in a coexisting multimodal wireless system. We show that the synchrosqueezing transform (SST) produces a highly localized TF representation but was a biased instantaneous frequency estimate (IFE) for high frequency modulation (FM) waveforms. This resulted in inaccurate instantaneous frequency (IF) estimation by the ridge extraction algorithm. The unbiased IFE matched to a linear frequency modulation (LFM) waveform was explored and applied to obtain accurate IF estimates. For a LFM wavefrom, we compare the performance of the modified SST (MSST) which uses the unbiased IFE matched to LFM with the biased SST for varying signal-to-noise ratios (SNR). The unbiased IFE matched to LFM performs exceedingly well when compared to biased IFE. The unbiased IFE mathced to a LFM is used to then compute MSST of a nonlinear frequency modulation (NFM) waveform like a power FM. For high SNR conditions, the unbiased IFE matched to LFM did perform better than the biased IFE. However, the unbiased IFE matched to LFM is a biased IFE for a NFM waveform model.

We proposed a new technique based on warping of NFM waveform. We demonstrate for a power FM waveform with unknown chirp rate, the signal can be warped to a LFM waveform by time-axis warping. Now that we have a LFM waveform after the warping operation, we can compute the MSST for the warped NFM waveform using the unbiased IFEs that are matched to LFM waveform. After estimation of

the IF using ridge extraction algorithm, the IF of the NFM can be computed using the reverse warping operator. We derive the conditions on the phase function of the NFM waveform for the above warping process to be possible.

5.2 Future Work

In this thesis we show the warping operation for a power FM, a future direction for IF estimation includes extending it to different nonlinear FM like a hyperbola. The MSST best matched to a LFM waveform can be used to increase the signal-to-interference-and-noise ratio at the radar receiver, where the communication users with LFM waveforms are observed as interference. In some signaling schemes, where the IF of the radar waveform intersects the IF of the communication users waveforms, and in order to estimate the IF of the radar waveform an adaptive technique can be developed to use the TF separation algorithm explored in this thesis, to be applied only in specific regions of the TF plane where only the radar waveform is present. To better estimate IF, a forward or backward smoothing operation can be considered to reduce the oscillatory behaviour of the TF representation at low frequency modulation regions.

REFERENCES

[1] J. S. Kota, "Transmit waveform design for coexisting radar and communications systems," Ph.D. dissertation, Arizona State University, 2016.

[2] K. Huang, M. Bică, U. Mitra, and V. Koivunen, "Radar waveform design in spectrum sharing environment: Coexistence and cognition," in *IEEE Radar Conference*, 2015, pp. 1698–1703.

[3] J. G. Metcalf, C. Sahin, S. D. Blunt, and M. Rangaswamy, "Analysis of symbol-design strategies for intrapulse radar-embedded communications," *IEEE Transactions on Aerospace and Electronic Systems*, vol. 51, pp. 2914–2931, 2015.

[4] J. Kota, N. Kovvali, D. W. Bliss, and A. Papandreou-Suppappola, "Waveform selection for range and Doppler estimation via Barankin bound signal-to-noise ratio threshold," in *IEEE Int. Conference on Acoustic, Speech, and Signal Processing*, May 2014, pp. 4658–4662.

[5] J. S. Kota, G. M. Jacyna, and A. Papandreou-Suppappola, "Radar waveform selection using estimation performance bounds under high communications interference conditions," *submitted to, IEEE Transactions on Signal Processing*, 2018.

[6] F. Auger, O. Lemoine, P. Gonçalvés, and P. Flandrin, "The time-frequency toolbox," June 1991. [Online]. Available: http://tftb.nongnu.org

[7] I. Daubechies and S. Maes, "A nonlinear squeezing of the continuous wavelet transform based on auditory nerve models," *Wavelets in Medicine and Biology*, pp. 527–546, 1996.

[8] G. Thakur and H.-T. Wu, "Synchrosqueezing based recovery of instantaneous frequency from nonuniform samples," *SIAM Journal on Mathematical Analysis*, vol. 43, pp. 2078–2095, 2011.

[9] G. Thakur, E. Brevdo, N. S. Fuckar, and H. T. Wu, "The synchrosqueezing algorithm for time-varying spectral analysis: Robustness properties and new paleoclimate applications," *Signal Processing*, vol. 93, pp. 1079–1094, 2013.

[10] T. Oberlin, S. Meignen, and V. Perrier, "The Fourier-based synchrosqueezing transform," *IEEE Int. Conference on Acoustics, Speech, and Signal Processing*, pp. 315–319, 2014.

[11] S. Meignen, T. Oberlin, and S. McLaughlin, "A new algorithm for multicompo-

nent signals analysis based on synchrosqueezing: With an application to signal sampling and denoising," *IEEE Transactions on Signal Processing*, vol. 60, pp. 5787–5798, 2012.

[12] I. Daubechies, J. Lu, and H. T. Wu, "Synchrosqueezed wavelet transforms: An empirical mode decomposition-like tool," *Applied and Computational Harmonic Analysis*, vol. 30, pp. 243–261, 2011.

[13] D. Fourer, F. Auger, K. Czarnecki, S. Meignen, and P. Flandrin, "Chirp rate and instantaneous frequency estimation: Application to recursive vertical synchrosqueezing," *IEEE Signal Processing Letters*, vol. 24, pp. 1724–1728, 2017.

[14] V. S. Gattani, J. S. Kota, and A. Papandreou-Suppappola, "Time-frequency separation of matched-waveform signatures of coexisting multimodal systems," in *Asilomar Conference on Signals, Systems and Computers*, October 2018.

[15] L. Cohen, *Time-frequency Analysis*. Prentice-Hall, 1995, ch. 7, pp. 93–110.

[16] A. Papandreou-Suppappola, *Applications in Time-Frequency Signal Processing*. CRC Press, 2003, ch. 1, pp. 1–84.

[17] J. B. Allen, "Short time spectral analysis, synthesis, and modification by discrete Fourier transform," *IEEE Transactions on Acoustics, Speech, and Signal Processing*, vol. 25, pp. 235–238, 1977.

[18] K. Kodera, C. deVilledary, and R. Gendrin, "A new method for the numerical analysis of non-stationary signals," *Phys. Earth Planetary Interiors*, vol. 12, pp. 142–150, 1976.

[19] F. Auger and P. Flandrin, "Improving the readability of time-frequency and time-scale representations by the reassignment method," *IEEE Transactions on Signal Processing*, vol. 43, pp. 1068–1089, 1995.

[20] P. Flandrin, "Time-frequency reassignment: From principles to algorithms," in *Applications in Time-Frequency Signal Processing*, A. Papandreou-Suppappola, Ed. CRC Press, 2003, ch. 5, pp. 179–204.

[21] F. Auger, E. Chassande-Mottin, and P. Flandrin, "Making reassignment adjustable: The Levenberg-Marquardt approach," in *IEEE Int. Conference on Acoustics, Speech, and Signal Processing*, 2012, pp. 3889–3892.

[22] D. Fourer, F. Auger, and P. Flandrin, "Recursive versions of the Levenberg-Marquardt reassigned spectrogram and of the synchrosqueezed STFT," *IEEE*

Int. Conference on Acoustic, Speech, and Signal Processing, pp. 4880–4884, 2016.

[23] F. Auger, P. Flandrin, Y. T. Lin, S. McLaughlin, S. Meignen, T. Oberlin, and H. T. Wu, "Time-frequency reassignment and synchrosqueezing: An overview," *IEEE Signal Processing Magazine*, vol. 30, pp. 32–41, 2013.

[24] R. A. Carmona, W. L. Hwang, and B. Torrésani, "Characterization of signals by the ridges of their wavelet transforms," *IEEE Transactions on Signal Processing*, vol. 45, pp. 2586–2590, 1997.

[25] R. A. Carmona, W. L. Hwang, and B. Torrésani, "Multiridge detection and time-frequency reconstruction," *IEEE Transactions on Signal Processing*, vol. 47, pp. 480–492, 1999.

[26] S. Kirkpatrick, C. D. Gelatt Jr, and M. P. Vecchi, "Optimization by simulated annealing," *Science*, vol. 220, pp. 671–680, 1983.

[27] T. Oberlin, S. Meignen, and V. Perrier, "Second-order synchrosqueezing transform or invertible reassignment? towards ideal time-frequency representations," *IEEE Transactions on Signal Processing*, vol. 63, pp. 1335–1344, 2015.

[28] R. Behera, S. Meignen, and T. Oberlin, "Theoretical analysis of the second-order synchrosqueezing transform," *Applied and Computational Harmonic Analysis*, vol. 45, pp. 379–404, 2015.

[29] J. S. Kota, G. M. Jacyna, and A. Papandreou-Suppappola, ""nonstationary signal design for coexisting radar and communications systems," in *Asilomar Conference on Signals, Systems and Computers*, November 2016, pp. 549–553.

[30] A. Papandreou, F. Hlawatsch, and G. F. Boudreaux-Bartels, "The hyperbolic class of quadratic time-frequency representations part I: Constant-Q warping, the hyperbolic paradigm, properties, and members," *IEEE Transactions on Signal Processing*, vol. 41, pp. 3425–3444, 1993, special Issue on Wavelets and Signal Processing.

[31] A. Papandreou-Suppappola, "Generalized time-shift covariant quadratic time-frequency representations with arbitrary group delays," in *Asilomar Conference on Signals, Systems, and Computers*, 1995, pp. 553–557.

[32] A. Papandreou, F. Hlawatsch, and G. F. Boudreaux-Bartels, "Quadratic time-frequency representations with scale covariance and generalized time-shift covariance: A unified framework for the affine, hyperbolic and power classes," *Digital Signal Processing: A Review Journal*, vol. 8, pp. 3–48, 1998.

[33] F. Hlawatsch, A. Papandreou-Suppappola, and G. F. Boudreaux-Bartels, "The power classesquadratic time-frequency representations with scale covariance and dispersive time-shift covariance," *IEEE Transactions on Signal Processing*, vol. 47, pp. 3067–3083, 1999.

[34] R. G. Baraniuk, "Warped perspectives in time-frequency analysis," *Proceedings of IEEE-SP International Symposium on Time-Frequency and Time-Scale Analysis*, pp. 528–531, 1994.